



CHORUS

This is the accepted manuscript made available via CHORUS. The article has been published as:

Superradiance in spherical layered nanostructures

S. V. Goupalov

Phys. Rev. B **93**, 235302 — Published 9 June 2016

DOI: [10.1103/PhysRevB.93.235302](https://doi.org/10.1103/PhysRevB.93.235302)

Superradiance in Spherical Layered Nanostructures

S.V. Goupalov

Department of Physics, Jackson State University, Jackson, MS 39217 USA

and A.F. Ioffe Physico-Technical Institute,

26 Polytechnicheskaya, 194021 St. Petersburg, Russia

Abstract

We propose a design of a spherically symmetric nanostructure consisting of alternate concentric semiconductor and dielectric layers. The exciton states in different semiconductor layers of such a structure interact via the common electro-magnetic field of light. We show that, if the exciton states in N semiconductor layers are in resonance with one another, then a superradiant state emerges under optical excitation of such a structure. We discuss the conditions under which superradiance can be observed and show that they strongly depend on the valence-band structure of the semiconductor layers.

PACS numbers: 73.21.La, 78.67.Hc, 42.50.Nn, 78.67.Bf

I. INTRODUCTION

Superradiance is a phenomenon that occurs when a group of N dipole emitters interact with a common light field. It was first described in the pioneering article by Dicke [1] for a gas of atoms, confined within a volume with linear dimensions less than the wavelength of the radiated light. Dicke showed that, due to the mutual coupling between atoms through the electromagnetic field, the rate at which any one excited atom radiates is significantly influenced by the presence of all the other atoms. This phenomenon has been extensively discussed and experimentally observed for systems of free atoms [2–5], trapped ions [6], excitons in disordered π -conjugated polymers [7], artificial atoms represented by superconducting qubits coupled to a microwave cavity [8], Mössbauer nuclei [9], and an ensemble of individual quantum dots [10–13].

The superradiance phenomenon is usually considered in two different contexts, depending on its experimental realization. One realization [2–5, 8, 12] implies that the system, considered as an ensemble of two-level emitters is initially prepared in the state with a total population inversion. This totally inverted state is radiatively coupled to the completely symmetric linear combination of the states with $(N - 1)$ excited emitters. The latter state is radiatively coupled to the completely symmetric linear combination of the states with $(N - 2)$ excited emitters, *etc.* Thus, the system evolution appears as a cascade emission down a “ladder” of equidistant levels until it reaches the ground state [2–4]. As a result, the energy of the system is radiatively damped in a short radiation burst, within a time of the order of τ_0/N , where τ_0 is the radiative lifetime of a single emitter. We will call all the states participating in the system evolution according to this scenario “superradiant” although some authors [1, 3] reserve this term for the states with the population close to $N/2$ which have the shortest radiative lifetimes. Note, however, that in the case of two emitters the state which is a symmetric linear combination of the two states with one of the emitters in its excited and the other one in its ground state is superradiant in both senses.

The other realization [9–11, 13] is the case of the linear spectroscopy when the system is initially in its ground state and only the state with a single excited emitter is accessible in the linear regime. Yet, this state is a completely symmetric one, and its radiative lifetime, τ_0/N , is N times shorter than the lifetime of an individual emitter, τ_0 .

Parascandolo and Savona [10] employed the semiclassical model with nonlocal linear

response to describe interaction of the disc-shaped quantum dots with a common electromagnetic field. A complex geometry and low symmetry of the problem precluded them from obtaining analytical results. In this paper we will consider similar problem for a spherically symmetric system and will show that in this case the semiclassical model with nonlocal linear response allows one to derive simple analytical expressions, at least in the long-wavelength limit, and to gain some insight into the nature of the superradiant states and interaction of confined excitons with the common longitudinal and transverse electric fields.

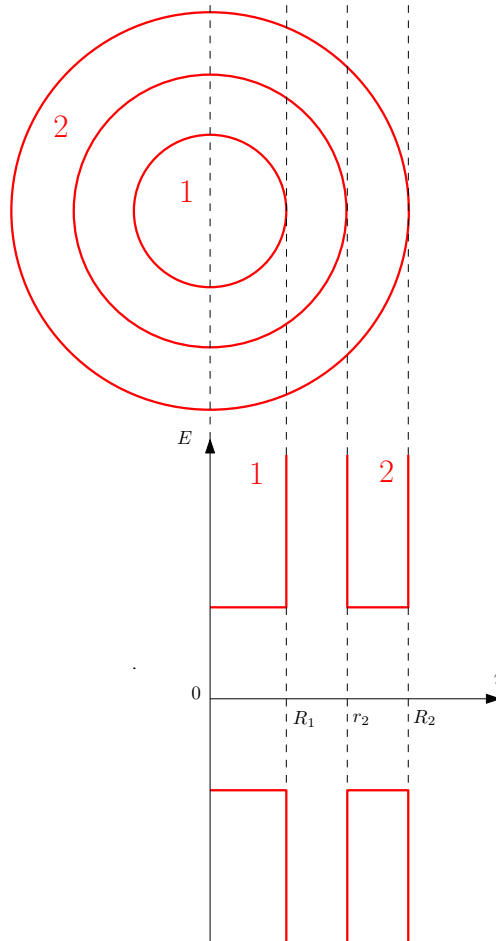


FIG. 1: (Color online). Scheme and energy band diagram of the proposed nanostructure with the two concentric spherical semiconductor layers labeled by the red numbers “1” (core) and “2” (outer shell) separated by a dielectric layer. The dielectric layer is shown to have an infinitely large band-gap to emphasize an absence of tunneling between the semiconductor layers.

To be more specific, we propose a design of a spherical layered onion-like nanostructure where the concentric spherical semiconductor layers which serve as light emitters are in-

terleaved with layers of another semiconductor or rather dielectric material having a wider band-gap (see Fig. 1). We assume that the difference in band-gaps between the semiconducting and dielectric layers is high enough to prevent tunneling between the exciton states in the semiconductor layers which remain connected only via the common field. We will show that, when the exciton energy levels in different semiconductor layers are in resonance with one another, a superradiant state emerges under optical excitation of such a structure. The total size of the structure should be small compared to the wavelength of light. To the best of our knowledge, the situation where superradiant states are formed by emitters of different geometry is being discussed here for the first time.

In recent years a great progress has been made in synthesizing multishell spherical semiconductor nanocrystals [14–19]. In particular, CdSe/ZnS/CdSe quantum-dot/quantum-shell structures having a CdSe core with diameter from 42 Å to 64 Å, followed by 3 or 4 monolayers of ZnS and several monolayers of CdSe and having wurtzite crystal structure have been synthesized [15–17]. Though the ZnS shell layer in these structures was probably too thin to completely prevent carriers from tunneling between the CdSe layers [16], the difference in band-gaps between bulk CdSe (1.74 eV) and ZnS (3.7 eV) is significant and these nanostructures have band diagrams very similar to the one shown in Fig. 1. However, this system lacks a certain flexibility because of the large (about 13 %) lattice mismatch between CdSe and ZnS which does not allow one to grow the ZnS shell of the CdSe/ZnS/CdSe nanocrystal thicker than five monolayers [15]. One may expect appearance of more flexible multishell nanostructures in the nearest future.

Exciton in a single quantum dot interacts not only with the transverse electro-magnetic field of light but also with a polarization-induced longitudinal electric field. The former interaction is responsible for the exciton radiative decay while the latter is equivalent to the electron-hole long-range (non-analytic) exchange interaction and leads to the exciton resonance frequency shift [20–25]. In the case of a spherical layered nanostructure, the transverse part of the electric field is responsible for the superradiance. We will show that, in the case of the semiconductor layers having a simple valence-band structure, the longitudinal electric field does not contribute to the inter-layer interaction. Therefore, different semiconductor layers serving as light emitters are coupled only radiatively while the system size might remain smaller than the wavelength of light. These are the conditions for superradiant systems originally proposed by Dicke [1]. When the semiconductor layers have a

complex valence-band structure then the inter-layer interaction is modified by the presence of the longitudinal electric field causing the dipole-dipole coupling between the emitters in addition to the radiative coupling.

Both synthesis of multishell semiconductor quantum dots [14–19] and spectroscopy of single nanocrystals [26–28] have advanced enough to enable experimental observation of superradiance in spherical layered nanostructures. However, to the best of our knowledge, no single-dot spectroscopy of colloidal multishell nanocrystals at cryogenic temperatures has been performed thus far. This paper seeks to inspire interest in studying superradiance in spherical layered nanostructures and provides some necessary theoretical background.

II. NANOSTRUCTURE WITH LAYERS OF SEMICONDUCTORS WITH SIMPLE BAND STRUCTURE

In this section we will consider an optical transition associated with the exciton formed by the electron and the hole from simple two-fold degenerate bands. One can consider the Γ_6 conduction band and the spin-orbitally split-off valence band Γ_7 of a cubic semiconductor of the crystal class T_d as an example. We will first consider a structure with the two light-emitting semiconductor layers and then generalize for an arbitrary number of layers. The difference in the dielectric permittivities of the layers will be neglected. We assume the strong confinement regime, so that the envelope of the exciton wave function is the product of the electron and hole envelopes. The high symmetry of the present problem allows for a fully analytic treatment. Taking into account the difference in dielectric permittivities of different layers presents no principal difficulty and can be readily done using the approaches outlined elsewhere [21] but would involve cumbersome expressions.

We will consider optical excitation on a frequency close to the exciton resonances. Then incident light induces the macroscopic linear polarization density associated with the excitonic resonances in the two semiconductor layers given by [20–22]

$$4\pi\mathbf{P}(\mathbf{r}) = \varepsilon_b \pi a_B^3 \omega_{LT} \left(\frac{\Phi_1(r) \boldsymbol{\Lambda}_1}{\omega_1 - \omega - i0} + \frac{\Phi_2(r) \boldsymbol{\Lambda}_2}{\omega_2 - \omega - i0} \right), \quad (1)$$

where ω_i is the frequency of the exciton resonance in the i -th semiconductor layer (neglecting corrections due to the electron-hole long-range exchange interaction [20–25]), ω is the frequency of light, ε_b is the background dielectric permittivity, a_B and ω_{LT} are the bulk exci-

ton Bohr radius and longitudinal-transverse splitting, respectively, and $\Phi_i(r)$ is the exciton envelope wave function in the i -th semiconductor layer taken at the coinciding coordinates of the electron and the hole. If tunneling is completely suppressed then $\Phi_1(r)$ is only different from zero for $0 \leq r < R_1$, where R_1 is the radius of the first (core) semiconductor layer (see Figure 1). In the same limit $\Phi_2(r)$ is only different from zero for $r_2 < r < R_2$, where r_2 and R_2 are, respectively, the inner and the outer radii of the second semiconductor layer. The vector Λ_i is related to the amplitude of the full Maxwell electric field $\mathbf{E}(\mathbf{r})$ by

$$\Lambda_i = \int d\mathbf{r} \Phi_i(r) \mathbf{E}(\mathbf{r}). \quad (2)$$

The Maxwell equations can be arranged in the form [21, 22]

$$(\Delta + k^2) \mathbf{E}(\mathbf{r}) = -k_0^2 4\pi \mathbf{P}(\mathbf{r}) - \varepsilon_b^{-1} \text{grad} [\text{div} (4\pi \mathbf{P}(\mathbf{r}))], \quad (3)$$

where $k_0 = \omega/c$, c is the speed of light, $k = \sqrt{\varepsilon_b} k_0$. Using Green's function of the Helmholtz equation, Eq. (3) can be written in the form

$$\mathbf{E}(\mathbf{r}) = \mathbf{E}^{(0)} e^{i\mathbf{k}\mathbf{r}} - \int d\mathbf{r}' \sum_{\alpha,\beta=x,y,z} 4\pi P_\beta(\mathbf{r}') \varepsilon_b^{-1} V^{-1} \sum_{\mathbf{q}} \frac{q_\alpha q_\beta - k^2 \delta_{\alpha,\beta}}{q^2 - k^2 - i0} e^{i\mathbf{q}(\mathbf{r}-\mathbf{r}')} \hat{\mathbf{e}}_\alpha, \quad (4)$$

where $\mathbf{E}^{(0)}$ is the amplitude of the electric field in the incident light, V is the normalization volume, and $\hat{\mathbf{e}}_\alpha$ is the unit vector along the Cartesian axis α . Multiplying Eq. (4) by $\Phi_1(r)$, $\Phi_2(r)$ and using Eq. (2) we obtain the following coupled algebraic equations

$$\Lambda_1 = \Lambda_1^{(0)} - \frac{\Xi^{1,1}}{\omega_1 - \omega - i0} \Lambda_1 - \frac{\Xi^{1,2}}{\omega_2 - \omega - i0} \Lambda_2, \quad (5)$$

$$\Lambda_2 = \Lambda_2^{(0)} - \frac{\Xi^{2,1}}{\omega_1 - \omega - i0} \Lambda_1 - \frac{\Xi^{2,2}}{\omega_2 - \omega - i0} \Lambda_2. \quad (6)$$

Here $\Lambda_i^{(0)} = \mathbf{E}^{(0)} \Phi_i(\mathbf{k})$, where $\Phi_i(\mathbf{k})$ is the Fourier transform of $\Phi_i(r)$,

$$\Xi^{i,j} = \frac{a_B^3 \omega_{LT}}{2\pi} \left[v.p. \int_0^\infty dq q^2 \Phi_i(\mathbf{q}) \Phi_j(\mathbf{q}) \frac{q^2/3 - k^2}{q^2 - k^2} - \frac{i\pi}{3} k^3 \Phi_i(\mathbf{k}) \Phi_j(\mathbf{k}) \right], \quad (7)$$

“*v.p.*” means the principal value of an integral, and we took into account that $\Phi_i(\mathbf{k})$ is real. Note that the matrix $\Xi^{i,j}$ is symmetric but not Hermitian.

Resolving Eqs. (5), (6) for *e.g.* Λ_1 we get the new, renormalized, values of the exciton resonant frequencies

$$\omega_{I,II} = \frac{\omega_1 + \omega_2 + \Xi^{1,1} + \Xi^{2,2}}{2} \pm \frac{1}{2} \sqrt{(\omega_1 + \Xi^{1,1} - \omega_2 - \Xi^{2,2})^2 + 4\Xi^{1,2}\Xi^{2,1}}. \quad (8)$$

The real parts of the diagonal elements $\Xi^{1,1}$ and $\Xi^{2,2}$ determine renormalization of the exciton resonance frequencies due to the long-range electron-hole exchange interaction [20–25]. Their imaginary parts determine exciton radiative lifetimes when the coupling between semiconductor layers via the electro-magnetic field is neglected [21–23]:

$$(2\tau_i)^{-1} = -\Im\Xi^{i,i} = \frac{a_B^3 \omega_{LT}}{6} k^3 [\Phi_i(\mathbf{k})]^2 \approx \frac{a_B^3 \omega_{LT}}{6} k^3, \quad (9)$$

where the last approximate equation corresponds to the long-wavelength limit. In this limit one can replace $\Phi_i(\mathbf{k})$ by $\Phi_i(\mathbf{q} = 0)$ and use the fact that, in the case of the simple valence band structure, the electron and hole envelope wave functions coincide. Then $\Phi_i(\mathbf{q} = 0) = 1$ due to the normalization condition. As a result, one can write $\tau_1 \approx \tau_2 \equiv \tau_0$. Indeed, if $\Xi^{1,2} = \Xi^{2,1} = 0$ in Eq. (8) then this equation yields the resonant frequencies $\omega_I = \omega_1 + \Xi^{1,1}$ and $\omega_{II} = \omega_2 + \Xi^{2,2}$ so that

$$\Im\omega_{I,II} = -(2\tau_0)^{-1}. \quad (10)$$

To analyze the effect of the coupling between the two exciton resonances via the electro-magnetic field of light it is enough to calculate the non-diagonal elements $\Xi^{1,2} = \Xi^{2,1}$ in the long-wavelength limit, when their real parts vanish:

$$\Xi^{1,2} = \Xi^{2,1} \approx -i \frac{a_B^3 \omega_{LT}}{6} k^3 \Phi_1(\mathbf{k}) \Phi_2(\mathbf{k}) \approx -i \frac{a_B^3 \omega_{LT}}{6} k^3 = -i (2\tau_0)^{-1}. \quad (11)$$

Disappearance of the real part of $\Xi^{1,2}$ can be seen from the fact that the Fourier transform of the term $q_\alpha q_\beta / q^2$ [cf. Eq. (4) at $k \rightarrow 0$] contains a term proportional to the coordinate delta-function and a term with a spatial dependence of the field of a dipole [24, 25, 29]. The former term does not contribute to the real part of $\Xi^{1,2}$ because $\Phi_1(r)$ and $\Phi_2(r)$ do not overlap, and the latter term does not contribute to it because $\Phi_1(r)$ and $\Phi_2(r)$ are independent of the angles. Note, however, that the imaginary parts of the diagonal and non-diagonal elements $\Xi^{i,j}$ coincide.

Now let us consider the case of the exact resonance between the two exciton states: $\omega_1 + \Xi^{1,1} = \omega_2 + \Xi^{2,2}$. Then Eq. (8) yields

$$\Im\omega_{I,II} = -(2\tau_0)^{-1} \mp (2\tau_0)^{-1}. \quad (12)$$

Therefore, we obtain one dark (subradiant, anti-superradiant) state and one superradiant state with the radiative lifetime $\tau = \tau_0/2$.

One can see from Eq. (8) that, in order for the superradiant state to emerge, the frequency detuning from the resonance condition should be no less than the spectral linewidth of the exciton level. Indeed, as soon as the first term under the sign of the square root in Eq. (8) becomes larger, by the absolute value, than the second one, the entire square root will have no effect on the imaginary parts of the renormalized frequencies.

Now let us generalize these results for the case of N semiconductor layers. Then, instead of Eqs. (5), (6), we will have

$$\Lambda_i = \Lambda_i^{(0)} - \sum_j \frac{\Xi^{i,j}}{\omega_j - \omega - i0} \Lambda_j, \quad (13)$$

where $i, j = 1, \dots, N$. If these equations are considered as a non-homogeneous system of linear equations on

$$\frac{\Lambda_j}{\omega_j - \omega - i0}$$

then one can formally resolve it using Cramer's rule. This yields the following equation for the resonant frequencies

$$\det \begin{vmatrix} \omega_1 + \Xi^{1,1} - \omega & \Xi^{1,2} & \dots & \Xi^{1,N} \\ \Xi^{2,1} & \omega_2 + \Xi^{2,2} - \omega & \dots & \Xi^{2,N} \\ \vdots & \vdots & \ddots & \vdots \\ \Xi^{N,1} & \Xi^{N,2} & \dots & \omega_N + \Xi^{N,N} - \omega \end{vmatrix} = 0 \quad (14)$$

or, equivalently,

$$\begin{aligned} \prod_{i=1}^N (\omega_i - \omega) + \sum_j \Xi^{j,j} \prod_{i \neq j} (\omega_i - \omega) + \sum_{j < k} \det \begin{vmatrix} \Xi^{j,j} & \Xi^{j,k} \\ \Xi^{k,j} & \Xi^{k,k} \end{vmatrix} \prod_{i \neq j,k} (\omega_i - \omega) \\ + \dots + \det \begin{vmatrix} \Xi^{1,1} & \dots & \Xi^{1,N} \\ \vdots & \ddots & \vdots \\ \Xi^{N,1} & \dots & \Xi^{N,N} \end{vmatrix} = 0. \end{aligned} \quad (15)$$

Indeed, for $N = 1$ one has $\omega_1 - \omega + \Xi^{1,1} = 0$, for $N = 2$ we obtain

$$(\omega_1 - \omega)(\omega_2 - \omega) + \Xi^{1,1}(\omega_2 - \omega) + \Xi^{2,2}(\omega_1 - \omega) + \Xi^{1,1}\Xi^{2,2} - \Xi^{1,2}\Xi^{2,1} = 0$$

which leads to Eq. (8). In the general case, Eq. (15) results from regrouping terms in a representation of the determinant, Eq. (14), in the form of a sum over all permutations of the numbers $1, 2 \dots N$.

In the case of an exact resonance between the exciton states in all the semiconductor layers one has $\omega_i + \Re \Xi^{i,i} = \omega_0$ and $\Xi^{i,j} = \Re \Xi^{i,i} \delta_{i,j} - i(2\tau_0)^{-1}$, where $\Re \Xi^{i,i}$ is the exciton resonant frequency renormalization due to the long-range electron-hole exchange interaction in the i -th semiconductor layer. However, since ω_i and $\Xi^{i,i}$ enter Eq. (14) only as a sum, $\omega_i + \Xi^{i,i} = \omega_0 - i(2\tau_0)^{-1}$, one can redefine $\omega_i = \omega_0$ and $\Xi^{i,j} = -i(2\tau_0)^{-1}$, and Eq. (15) will still be valid. Then all the determinants in Eq. (15) vanish and it immediately follows that

$$(\omega_0 - \omega)^{N-1} [\omega_0 - N i(2\tau_0)^{-1} - \omega] = 0, \quad (16)$$

which corresponds to one superradiant state with the lifetime $\tau = \tau_0/N$ and $N-1$ dark (sub-radiant, anti-superradiant) states. Note that an analogous situation occurs for a radiative state of exciton polaritons in a resonant Bragg structure of multiple quantum wells [30].

III. NANOSTRUCTURE WITH LAYERS OF CUBIC SEMICONDUCTORS WITH COMPLEX VALENCE BAND STRUCTURE

In Sec. II we considered a situation when the coupling between the semiconductor layers is only due to the transverse part of the electric field. As a result, $\Xi^{1,2}$ is purely imaginary and has no real part. In this case the expression under the sign of square root in Eq. (8) is always real, and the square root can only acquire an imaginary part as a result of this expression being negative. This narrows the conditions under which the superradiance can be observed to a very sharp resonance between the exciton energy levels in the two semiconductor layers. The width of this resonance is determined by the exciton radiative lifetime. The situation changes drastically if $\Xi^{1,2}$ has an appreciable real part. In this case the square root in Eq. (8) will always have some imaginary part, no matter how large is the detuning from the resonant conditions. We will see that this is the case of the semiconductor layers made of a material with the complex valence band structure. It happens because, for the valence band described by the Luttinger effective Hamiltonian, the envelope of the ground state wave function of the confined hole will contain an angular-dependent part characterized by the orbital angular momentum $L = 2$, and the coupling between the semiconductor layers via the longitudinal electric field will be no longer forbidden by the symmetry.

Indeed, the hole states near the extremum of the valence band Γ_8 can be characterized by the pseudo-spin angular momentum $J = 3/2$ (cf. Appendix B). The states of the confined

hole in a spherically symmetric semiconductor layer can be labeled by the values, F , of the total angular momentum which is the vector sum of the pseudo-spin and the orbital angular momentum. As, in our problem, this hole is left in the valence band as a result of the radiative transition, its wave function should contain an s -like part described by the orbital angular momentum $L = 0$. From the rule for addition of angular momenta one concludes that such state of the confined hole (in particular, its ground state) is characterized by the total angular momentum $F = 3/2$. But the same rule dictates that the even state having both $J = 3/2$ and $F = 3/2$ contains orbital contributions not only of $L = 0$, but also of $L = 2$.

A. Resonant Frequency Renormalization in a Nanostructure with Two Semiconductor Layers

We now turn our attention to details. We consider a layered spherical nanostructure with semiconductor layers having a cubic crystalline structure of the class T_d and a valence band of the Γ_8 symmetry described by the spherical Luttinger Hamiltonian [22], i.e., it is assumed that the Luttinger parameters $\gamma_2 = \gamma_3 \equiv \gamma$.

Core/shell nanocrystals with a zinc-blende structure CdSe core can be synthesized using the methods of colloidal chemistry [26, 31, 32], but, in fact, the theory developed in this section can be applied to the exciton states in wurtzite structure nanocrystals polarized along the C_6 axis. Besides, the only experimental observation of superradiance for ensembles of quantum dots we are aware of [11] was done for CdSe self-assembled quantum dots. Therefore, we will stick to CdSe parameters (see Appendix C) for the semiconductor layers in our numerical calculations.

In this section we will need wave functions for the ground states of the electron and the hole confined within a spherical layer with the inner radius r_2 and the outer radius R_2 . They are given in the Appendices. The following notations are used: $\alpha = r_2/R_2$, $\beta = (\gamma_1 - 2\gamma)/(\gamma_1 + 2\gamma)$. Below we will also use the notations $\alpha_2 \equiv \alpha$ and $\alpha_1 = 0$.

It is convenient to consider the incident light to be circularly polarized or linearly polarized along the z axis. In this case the optically excited exciton state can be characterized by the projection, \mathcal{F}_z , of the exciton total angular momentum onto the quantization axis, z . For exciton states optically active in the dipole approximation one has $\mathcal{F} = 1$. Therefore,

the exciton wave function in the j -th layer can be written with the help of the Wigner $3jm$ -symbol [20]:

$$|exc, \mathcal{F}_z, j\rangle = (-1)^{1+\mathcal{F}_z} \sqrt{3} \sum_{m,n} \begin{pmatrix} \frac{3}{2} & \frac{1}{2} & 1 \\ \mathcal{F}_z - m & m & -\mathcal{F}_z \end{pmatrix} \phi^{(\alpha_j)}(r_e/R_j, R_j) \quad (17)$$

$$\times \mathcal{R}_{n, \mathcal{F}_z - m}^{(\alpha_j)}(\mathbf{r}_h, R_j) |\Gamma_6, m\rangle |\Gamma_8, n\rangle,$$

where $|\Gamma_6, m\rangle$ and $|\Gamma_8, n\rangle$ are the Bloch functions in the conduction and the valence bands, $m = \pm 1/2$, $n = \pm 3/2, \pm 1/2$, and the functions $\phi^{(\alpha_j)}(r_e/R_j, R_j)$, $\mathcal{R}_{n, \mathcal{F}_z - m}^{(\alpha_j)}(\mathbf{r}_h, R_j)$ are introduced in the Appendices.

The complex conjugated covariant cyclic σ -component ($\sigma = \pm 1, 0$) of the dipole moment density matrix element between the ground state of the j -th semiconductor layer and the exciton can be written as [20]

$$\langle 0 | \hat{d}_\sigma^*(\mathbf{r}) | exc, 1\mathcal{F}_z, j \rangle = - \sum_{m,n} \frac{ie\hbar}{m_0 E_g} \langle \bar{n} | p_\sigma^* | m \rangle \Phi_{mn}^{j, 1\mathcal{F}_z}(\mathbf{r}), \quad (18)$$

where e is the electron charge, m_0 is the free-electron mass, E_g is the band gap energy, $\langle \bar{n} | p_\sigma^* | m \rangle$ is the matrix element of the complex conjugated covariant cyclic σ -component ($\sigma = \pm 1, 0$) of the momentum operator calculated between the electron Bloch functions $|m, \mathbf{k} = 0\rangle$ and $|\bar{n}, \mathbf{k} = 0\rangle$ (the hole state n, \mathbf{k} and the electron state $\bar{n}, -\mathbf{k}$ are related through time-reversal operation), and

$$\Phi_{mn}^{j, 1\mathcal{F}_z}(\mathbf{r}) = (-1)^{1+\mathcal{F}_z} \sqrt{3} \varphi^{(\alpha_j)}\left(\frac{r}{R_j}, R_j\right) \begin{pmatrix} \frac{3}{2} & \frac{1}{2} & 1 \\ \mathcal{F}_z - m & m & -\mathcal{F}_z \end{pmatrix} \mathcal{R}_{n, \mathcal{F}_z - m}^{(\alpha_j)}(\mathbf{r}, R_j). \quad (19)$$

Note that

$$\langle \bar{n} | p_\sigma^* | m \rangle = 2 p_{cv} (-1)^{1-\sigma} \begin{pmatrix} \frac{1}{2} & \frac{3}{2} & 1 \\ m & n & -\sigma \end{pmatrix}, \quad (20)$$

where $p_{cv} = i \langle S | \hat{p}_x | X \rangle$ is the interband matrix element of the momentum operator.

The integral equation analogous to Eq. (4) can be written as

$$E^\sigma(\mathbf{r}) = E^{\sigma(0)}(\mathbf{r}) - \int d\mathbf{r}' \sum_{\mu} G_{\mu}^{\sigma}(\mathbf{r}, \mathbf{r}') 4\pi P^{\mu}(\mathbf{r}') \quad (21)$$

with

$$G_{\mu}^{\sigma}(\mathbf{r}, \mathbf{r}') = \varepsilon_b^{-1} V^{-1} \sum_{\mathbf{q}} \frac{(-1)^{\sigma} q_{-\sigma} q_{\mu} - k^2 \delta_{\sigma, \mu}}{q^2 - k^2 - i0} e^{i\mathbf{q}(\mathbf{r}-\mathbf{r}')}.$$

The amplitude of the contravariant cyclic μ -component of the polarization density in the rotating wave approximation is given by [20]

$$P^\mu(\mathbf{r}) = \frac{\hbar^{-1}\Lambda_1}{\omega_1 - \omega} \left\langle 0 \left| \hat{d}_\mu^*(\mathbf{r}) \right| exc, 1\mathcal{F}_z, j = 1 \right\rangle + \frac{\hbar^{-1}\Lambda_2}{\omega_2 - \omega} \left\langle 0 \left| \hat{d}_\mu^*(\mathbf{r}) \right| exc, 1\mathcal{F}_z, j = 2 \right\rangle, \quad (22)$$

where

$$\Lambda_j = \int d\mathbf{r} \sum_\sigma \left\langle exc, 1\mathcal{F}_z, j \left| \hat{d}_\sigma(\mathbf{r}) \right| 0 \right\rangle E^\sigma(\mathbf{r}).$$

This leads to the equations

$$\Lambda_1 = \Lambda_1^{(0)} - \frac{\Xi^{1,1}}{\omega_1 - \omega - i0} \Lambda_1 - \frac{\Xi^{1,2}}{\omega_2 - \omega - i0} \Lambda_2, \quad (23)$$

$$\Lambda_2 = \Lambda_2^{(0)} - \frac{\Xi^{2,1}}{\omega_1 - \omega - i0} \Lambda_1 - \frac{\Xi^{2,2}}{\omega_2 - \omega - i0} \Lambda_2 \quad (24)$$

with

$$\Xi^{i,j} = \frac{4\pi}{\hbar} \sum_\sigma \sum_\mu \int d\mathbf{r} \int d\mathbf{r}' G_\mu^\sigma(\mathbf{r}, \mathbf{r}') \left\langle exc, 1\mathcal{F}_z, i \left| \hat{d}_\sigma(\mathbf{r}) \right| 0 \right\rangle \left\langle 0 \left| \hat{d}_\mu^*(\mathbf{r}') \right| exc, 1\mathcal{F}_z, j \right\rangle \quad (25)$$

and

$$\Lambda_j^{(0)} = \int d\mathbf{r} \sum_\sigma \left\langle exc, 1\mathcal{F}_z, j \left| \hat{d}_\sigma(\mathbf{r}) \right| 0 \right\rangle E^{(0)\sigma}(\mathbf{r}).$$

After a straightforward derivation (cf. Ref. [20]) one obtains the following expressions for the real and the imaginary parts of $\Xi^{i,j}$, valid in the long-wavelength limit:

$$\Re \Xi^{i,j} = \frac{(1 - \delta_{ij}) \omega_{LT}}{18\pi^2} \left(\frac{a_B}{R_j} \right)^3 \int_0^\infty dy y^2 \left[I_0^{(\alpha_i)} \left(y \frac{R_i}{R_j} \right) I_2^{(\alpha_j)}(y) + I_2^{(\alpha_i)} \left(y \frac{R_i}{R_j} \right) I_0^{(\alpha_j)}(y) \right] + \Re \Xi^{i,i} \delta_{ij}, \quad (26)$$

$$\Re \Xi^{i,i} = \frac{\omega_{LT}}{18\pi^2} \left(\frac{a_B}{R_i} \right)^3 \int_0^\infty dy y^2 \left[I_0^{(\alpha_i)}(y) + I_2^{(\alpha_i)}(y) \right]^2. \quad (27)$$

$$\Im \Xi^{i,j} = -\frac{\omega_{LT} a_B^3 k^3}{18\pi} I_0^{(\alpha_i)}(0) I_0^{(\alpha_j)}(0), \quad (28)$$

where

$$\omega_{LT} = \frac{4\hbar}{\varepsilon_b a_B^3} \left(\frac{ep_{cv}}{m_0 E_g} \right)^2, \quad (29)$$

$$I_L^{(\alpha_j)}(y) = \frac{2\sqrt{2\pi}(-1)^{L/2}}{\sqrt{1-\alpha_j}} \cos \frac{\pi\alpha_j}{1-\alpha_j} \int_{\alpha_j}^1 dx x f_L^{(\alpha_j)}(x) j_L(xy) \\ \times \left[\sin \frac{\pi x}{1-\alpha_j} - \tan \frac{\pi\alpha_j}{1-\alpha_j} \cos \frac{\pi x}{1-\alpha_j} \right].$$

The renormalized resonant frequencies are still given by Eq. (8).

Note that the signs of the real and imaginary parts of the non-diagonal matrix elements $\Re \Xi^{1,2} = \Re \Xi^{2,1}$, $\Im \Xi^{1,2} = \Im \Xi^{2,1}$ depend on the choice of the phases of the wave functions (A1), (B2). However, the sign of their product is defined unambiguously. In what follows it is convenient to introduce positive quantities $\delta\omega_j$, V_{12} , and Γ_j , and, without loss of generality, set

$$\Xi^{j,j} = \delta\omega_j - i\Gamma_j/2, \quad (30)$$

$$\Xi^{1,2} = V_{12} - i\sqrt{\Gamma_1\Gamma_2}/2 \quad (31)$$

[cf. Eqs. (26), (27), (28)].

Let us fix the core radius, $R_1 = 20 \text{ \AA}$ and the outer radius of the second semiconductor layer, $R_2 = 60 \text{ \AA}$ and change its inner radius, r_2 , and, therefore, the parameter α . The energy difference of the exciton levels in the first, or core, and the second semiconductor layers is plotted as a function of α in Fig. 2, c. While calculating this energy difference, or detuning from the resonant conditions, we neglected a small contribution coming from the difference in the exciton binding energies. The energy positions of the two levels as functions of the detuning are shown in Fig. 2, d. The exciton level in the core layer almost does not change with the detuning which is due to the change of the energy position of the exciton state in the second semiconductor layer. However, close to the resonance one can see the avoided crossing of the two levels (see Fig. 2, a). The imaginary parts of the renormalized resonant frequencies are plotted in Fig. 2, b as functions of the detuning. The imaginary part of one of the renormalized frequencies drops to zero at zero detuning while the imaginary part of the second renormalized frequency increases, by the absolute value, as the sum of the imaginary parts of the two transition frequencies far from the resonance. This corresponds to the superradiance. Note the difference in the horizontal and vertical scales in Fig. 2, b. The width of the resonance in Fig. 2, b is more than two orders of magnitude larger than the imaginary parts of the resonant frequencies determining the exciton radiative linewidths. This is in contrast with the situation that we had in Sec. II and indicates favorable conditions for experimental observation of the superradiance in nanostructures of the proposed design using the methods of the single quantum dot spectroscopy [26–28]. As we emphasized above, the difference with the case of the nanostructure with semiconductor layers having a simple valence band structure considered in Sec. II is due to the fact that $\Re \Xi^{1,2}$ is no longer zero.

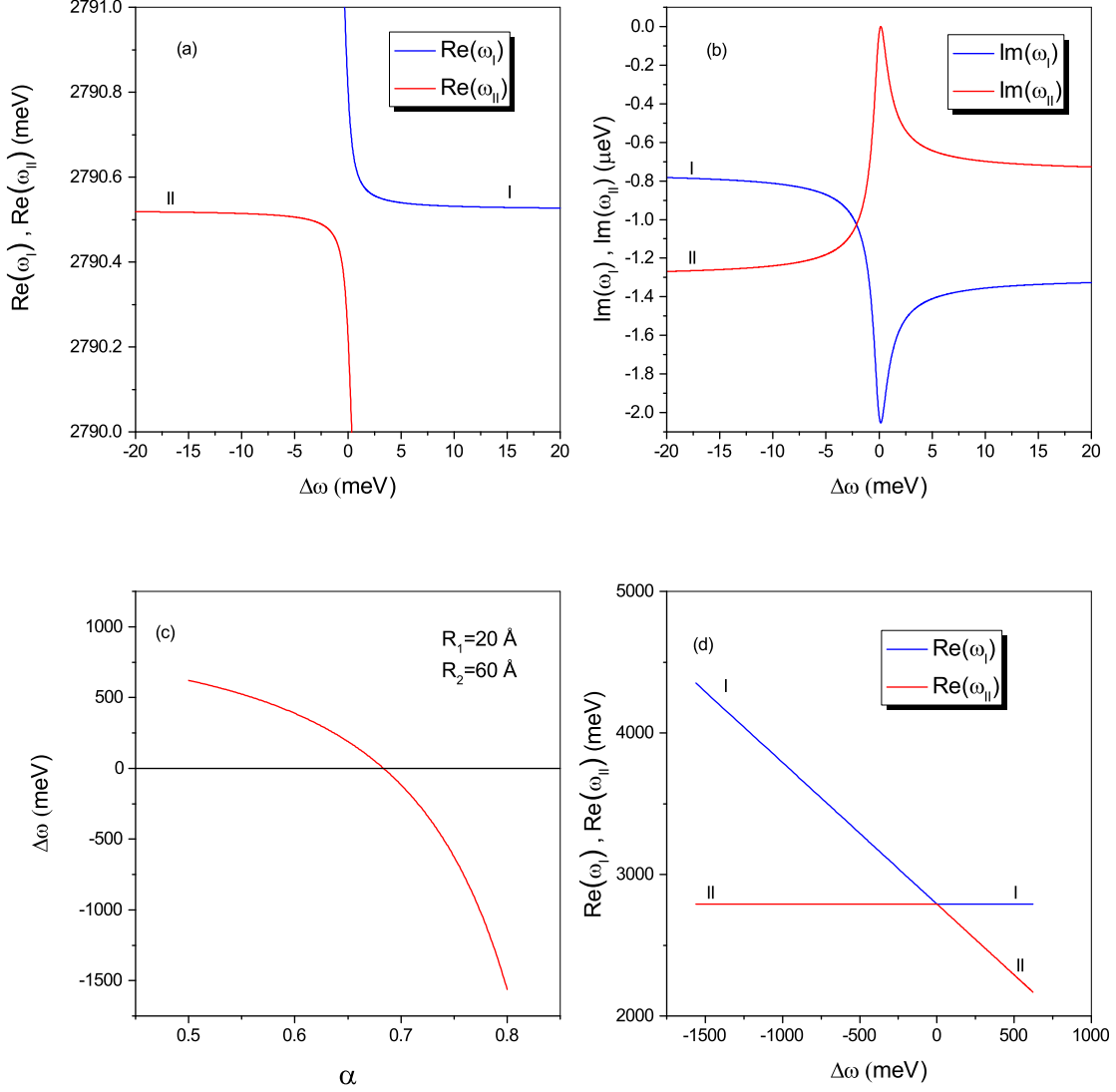


FIG. 2: (Color online). Emergence of superradiant state in a structure with two layers of cubic semiconductor: (a) Real parts of the renormalized frequencies as functions of the detuning from the resonance conditions. (b) Imaginary parts of the renormalized frequencies as functions of the detuning. (c) The detuning as a function of the parameter α . The inset specifies the structure sizes used in the calculation. (d) Same as (a) but scaled differently.

In Fig. 3 we plot the real and imaginary parts of $\Xi^{i,j}$ as functions of α for the same set of parameters that were used for Fig. 2. Their physical meaning is revealed in Sec. III B where we use notations introduced in Eqs. (30), (31).

Fig. 3 demonstrates that the real parts of the matrix elements $\Xi^{i,j}$ are two orders of magnitude larger than their imaginary parts. This allows one to make the corresponding

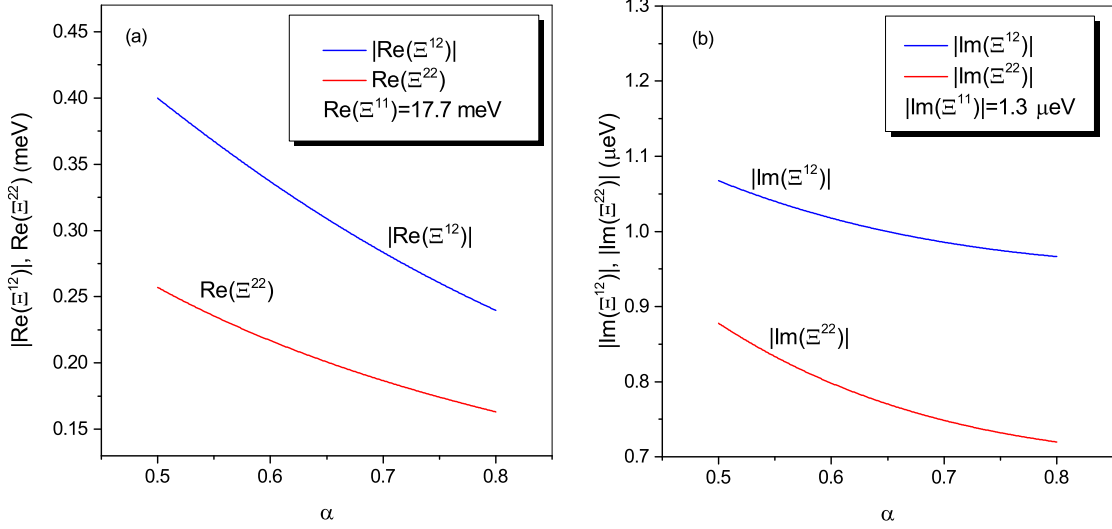


FIG. 3: (Color online). (a) Real parts of $\Xi^{1,2}$ and $\Xi^{2,2}$ as functions of the parameter α . The real part of $\Xi^{1,2}$ is shown by the absolute value. The value of the α -independent $\Re \Xi^{1,1}$ is shown in the inset. (b) Absolute values of the imaginary parts of $\Xi^{1,2}$ and $\Xi^{2,2}$ as functions of the parameter α . The value of the α -independent $\Im \Xi^{1,1}$ is shown in the inset.

expansion under the square root of Eq. (8). Using Eqs. (30), (31) and introducing $\Delta\omega = \omega_1 + \delta\omega_1 - \omega_2 - \delta\omega_2$ we obtain

$$\begin{aligned} \omega_{I,II} &= \frac{\omega_1 + \delta\omega_1 + \omega_2 + \delta\omega_2}{2} \pm \frac{1}{2} \sqrt{\Delta\omega^2 + 4V_{12}^2} \\ -i \frac{\Gamma_1 + \Gamma_2}{4} \mp i \frac{V_{12} \sqrt{\Gamma_1 \Gamma_2}}{\sqrt{\Delta\omega^2 + 4V_{12}^2}} \mp i \frac{\Delta\omega (\Gamma_1 - \Gamma_2)}{4 \sqrt{\Delta\omega^2 + 4V_{12}^2}}. \end{aligned} \quad (32)$$

One can see that Eq. (32) describes the behavior of the renormalized frequencies with the detuning shown in Figs. 2, a, b and shows explicitly that the width of the resonance in Fig. 2, b is on the order of $2V_{12}$. Also note that the difference between $2(\Gamma_1 + \Gamma_2)$ and $(\sqrt{\Gamma_1} + \sqrt{\Gamma_2})^2$ is of the second order in $(\Gamma_1 - \Gamma_2)$.

B. Dynamics of the Superradiant State

In order to study dynamics of the superradiant state we will introduce the states $|1\rangle \equiv |e_1, g_2\rangle$, where the exciton in the first semiconductor layer is excited while the second semiconductor layer is in its ground state, and its counterpart $|2\rangle \equiv |g_1, e_2\rangle$, where the exciton is in the second semiconductor layer. One can derive equations for the density matrix

in the basis of these states as well as the ground state $|0\rangle \equiv |g_1, g_2\rangle$ needed to preserve normalization: $\rho_{00} + \rho_{11} + \rho_{22} = 1$. These equations are analogous to the Optical Bloch Equations in the theory of two-level atoms [33, 34]. The field of the spontaneous radiation can be treated as a reservoir while the system evolution under the dipole-dipole interaction alone (which plays the role of the monochromatic incident radiation in the Optical Bloch Equation) is governed by the Schrödinger equation [33]. The resulting equations take the form

$$\frac{d\rho_{11}}{dt} = -\Gamma_1 \rho_{11} + i \left(V_{12} + i \frac{\sqrt{\Gamma_1 \Gamma_2}}{2} \right) \rho_{12} - i \left(V_{12} - i \frac{\sqrt{\Gamma_1 \Gamma_2}}{2} \right) \rho_{21}, \quad (33)$$

$$\frac{d\rho_{22}}{dt} = -\Gamma_2 \rho_{22} - i \left(V_{12} - i \frac{\sqrt{\Gamma_1 \Gamma_2}}{2} \right) \rho_{12} + i \left(V_{12} + i \frac{\sqrt{\Gamma_1 \Gamma_2}}{2} \right) \rho_{21}, \quad (34)$$

$$\frac{d\rho_{12}}{dt} = \left[-i \Delta\omega - \frac{\Gamma_1 + \Gamma_2}{2} \right] \rho_{12} + i \left(V_{12} + i \frac{\sqrt{\Gamma_1 \Gamma_2}}{2} \right) \rho_{11} - i \left(V_{12} - i \frac{\sqrt{\Gamma_1 \Gamma_2}}{2} \right) \rho_{22}, \quad (35)$$

$$\frac{d\rho_{21}}{dt} = \left[i \Delta\omega - \frac{\Gamma_1 + \Gamma_2}{2} \right] \rho_{21} - i \left(V_{12} - i \frac{\sqrt{\Gamma_1 \Gamma_2}}{2} \right) \rho_{11} + i \left(V_{12} + i \frac{\sqrt{\Gamma_1 \Gamma_2}}{2} \right) \rho_{22}. \quad (36)$$

These equations can be derived following the procedure outlined in Ref. [33]. Here they are given for zero temperature. Comparison with the Optical Bloch Equations shows that $2V_{12}$ is analogous to the Rabi frequency.

The system of Eqs. (33) – (36) can be solved analytically but we will restrict our consideration to an analysis of some limiting cases of the corresponding eigenfrequencies.

When $\Delta\omega = 0$ and $\Gamma_1 = \Gamma_2$ the eigenfrequencies are 0 , $-2i\Gamma_1$, and $\pm 2V_{12} - i\Gamma_1$. The first two eigenfrequencies correspond to the anti-superradiant and superradiant states, respectively, while the other two eigenvalues describe the damped Rabi oscillations. The renormalized frequencies of Eq. (8) are in this case $\omega_{II} = \omega_1 + \delta\omega_1 - V_{12}$ and $\omega_I = \omega_1 + \delta\omega_1 + V_{12} - i\Gamma_1$.

When $\Delta\omega = 0$ and $V_{12} = 0$ the eigenfrequencies are 0 , $-i\Gamma_1 - i\Gamma_2$, and a two-fold degenerate value $-i(\Gamma_1 + \Gamma_2)/2$. Clearly, the first two eigenvalues correspond to the anti-superradiant and superradiant states, respectively. The renormalized frequencies of Eq. (8) are in this case $\omega_{II} = \omega_1 + \delta\omega_1$ and $\omega_I = \omega_1 + \delta\omega_1 - i(\Gamma_1 + \Gamma_2)/2$.

When $V_{12} = 0$ and $\Gamma_1 = \Gamma_2$ the eigenfrequencies are $-i\Gamma_1 \pm \sqrt{\Delta\omega^2 - \Gamma_1^2}$, and a two-fold degenerate value $-i\Gamma_1$. The renormalized frequencies of Eq. (8) are in this case $\omega_{I,II} = (\omega_1 + \delta\omega_1 + \omega_2 + \delta\omega_2)/2 - i\Gamma_1/2 \pm \sqrt{\Delta\omega^2 - \Gamma_1^2}/2$.

Finally, when $\Gamma_1 = \Gamma_2 = 0$, we obtain a well-known set of the eigenfrequencies of the Optical Bloch Equations without damping [34]: a two-fold degenerate zero value

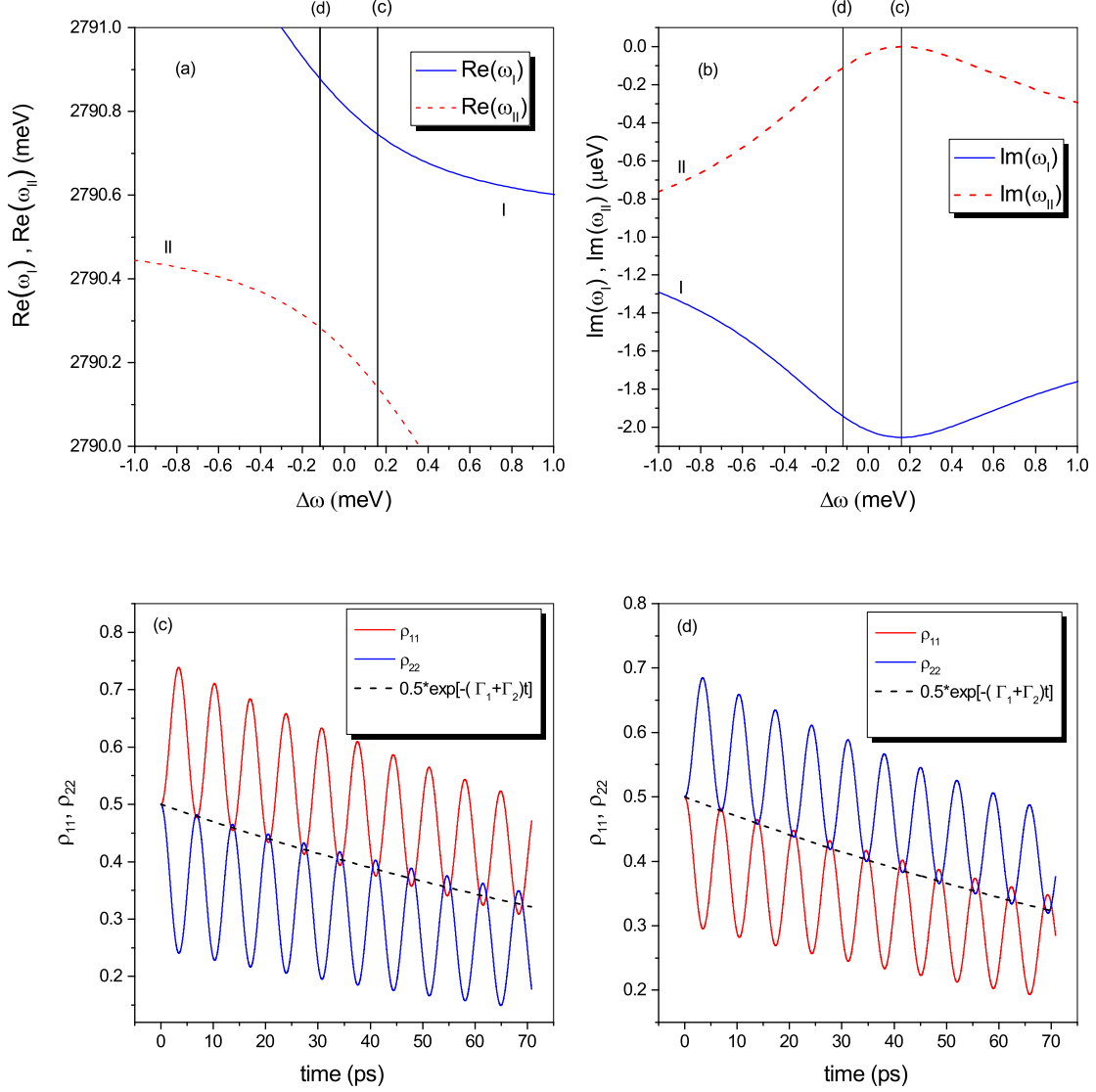


FIG. 4: (Color online). Dynamics of the superradiant state: (a),(b) Same as Fig. 2, a, b but scaled differently. The vertical lines marked as “(c)” and “(d)” indicate frequency detunings used as parameters for panels (c) and (d), respectively. (c),(d) The time dependences of ρ_{11} and ρ_{22} for the initial conditions of $\rho_{11}(0) = \rho_{22}(0) = \rho_{12}(0) = \rho_{21}(0) = 0.5$ and frequency detunings indicated in panels (a) and (b). Also shown is the time dependence of $0.5 \exp[-(\Gamma_1 + \Gamma_2)t]$.

and $\pm\sqrt{\Delta\omega^2 + 4V_{12}^2}$. The renormalized frequencies of Eq. (8) are in this case $\omega_{I,II} = (\omega_1 + \delta\omega_1 + \omega_2 + \delta\omega_2)/2 \pm \sqrt{\Delta\omega^2 + 4V_{12}^2}/2$.

Note that Eqs. (33) – (36), complemented by the phenomenological terms describing the decay of the “coherences” ρ_{12}, ρ_{21} with the transverse relaxation time, can be used to describe the Förster resonant energy transfer between semiconductor layers [35]. Such processes were

discussed in Ref. [15] for the CdSe/ZnS/CdSe multishell structures. While superradiance is a coherent phenomenon, the Förster resonant energy transfer is characterized by a short transverse relaxation time and is strictly incoherent [35].

In Fig. 4 we study time evolution of the system which can be initially found in both semiconductor layers with equal probability [$\rho_{11}(0) = \rho_{22}(0) = \rho_{12}(0) = \rho_{21}(0) = 0.5$] for two different energy differences between the excitons in the two layers. In both cases we see strong Rabi oscillations of the populations while the overall population decay is close to the “superradiant” exponent $\exp[-(\Gamma_1 + \Gamma_2)t]$, in agreement with Fig. 4, b. According to Fig. 4, a, the “superradiant” state corresponding to Fig. 4, c has energy closer to the level in the first semiconductor layer, as compared to the state corresponding to Fig. 4, d. This is consistent with the fact that the mean probability to find the system in the first semiconductor layer is higher than the mean probability to find the system in the second semiconductor layer for Fig. 4, c and lower for Fig. 4, d.

C. Nanostructure with Three Semiconductor Layers

Next we consider superradiance in a structure with three semiconductor layers. We take the structure with the two layers tuned to the conditions where one can observe superradiance (we take $R_1 = 20 \text{ \AA}$, $R_2 = 60 \text{ \AA}$, $\alpha_2 = 0.6835575$, cf. Fig. 2), and add an extra semiconductor layer with the outer radius $R_3 = 90 \text{ \AA}$. Then we change the ratio $\alpha_3 = r_3/R_3$, where r_3 is the inner radius of the third layer, and tune up the exciton level in the third layer into resonance with these in the first two semiconductor layers.

The renormalized resonant frequencies are given by the roots of Eq. (14) with $N = 3$ while the matrix elements $\Xi^{i,j}$ are determined by Eqs. (26), (27), and (28). The frequency detuning is defined as $\Delta\omega = \omega_1 + \Re\Xi^{1,1} - \omega_3 - \Re\Xi^{3,3}$.

The results are shown in Fig. 5. The resonance with the two-emitter anti-superradiant state has no effect on either the real or the imaginary part of the renormalized frequencies while the resonance with the two-emitter superradiant state clearly leads to an emergence of the three-emitter superradiant state.

If the first and the second semiconductor layers were off the resonant conditions for superradiance then we would also obtain an avoided crossing of levels I and II in Fig. 5, d. These conditions are not affected by the presence of the third semiconductor layer, as the

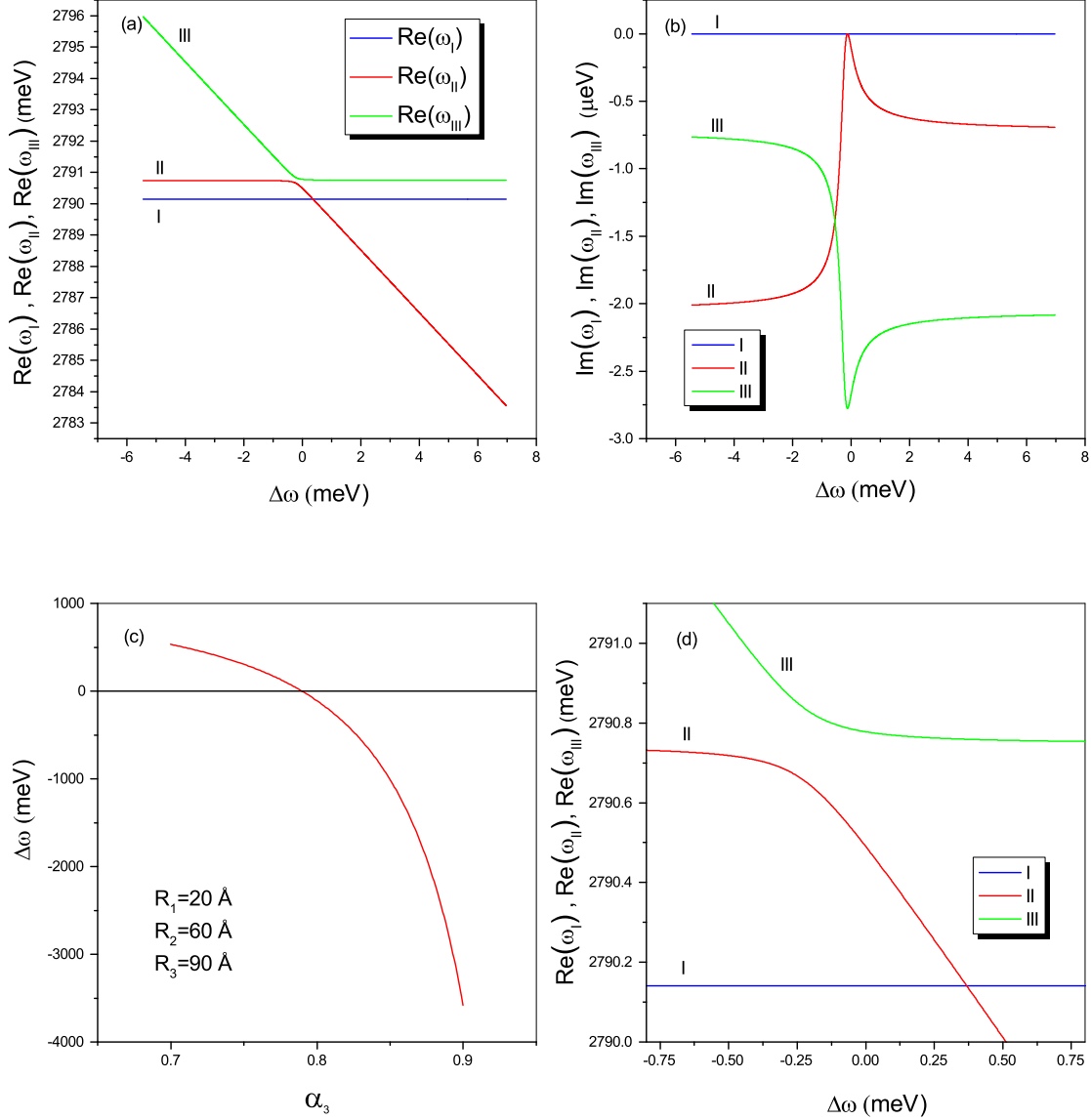


FIG. 5: (Color online). Emergence of superradiant state in a structure with three layers of cubic semiconductor: (a) Real parts of the renormalized frequencies as functions of the detuning from the resonance conditions. (b) Imaginary parts of the renormalized frequencies as functions of the detuning. (c) The detuning as a function of the parameter α_3 . The inset specifies the structure sizes used in the calculation. (d) Same as (a) but scaled differently.

dipole-dipole interaction between the first and the third semiconductor layers is negligible as compared to the dipole-dipole interactions between the first two and between the second two semiconductor layers. At the same time the radiative coupling between all the layers remains long-range on this scale.

IV. NANOSTRUCTURE WITH LAYERS OF WURTZITE SEMICONDUCTORS

In this section we will discuss nanostructures with the two semiconductor layers having wurtzite crystal lattice. This is the crystal lattice of bulk CdSe. CdSe nanocrystals with wurtzite crystal structure are more common than these with zinc-blende structure, and CdSe/ZnS/CdSe multishell nanocrystals studied in Refs. [15–17] also had wurtzite crystal structure. We will assume that the directions of the C_6 axes in both semiconductor layers coincide and consider circularly polarized light exciting the exciton states with the total angular momentum projection onto the wurtzite axis equal to +1.

The valence-band subbands of the light and heavy holes are split at the Γ -point of the Brillouin zone of a bulk semiconductor with wurtzite crystal lattice. Such valence-band structure is usually described by the spherical Luttinger Hamiltonian perturbed by the crystal field accounting for the splitting. For excitons in nanocrystals this splitting results in appearance of two exciton levels characterized by the total angular momentum projection onto the wurtzite axis equal to +1. We will distinguish the states in the j -th layer by the superscript: $+1^{U_j}$ and $+1^{L_j}$. The splitting between the two levels is further modified by the short-range (analytic) electron-hole exchange interaction [36]. The long-range (non-analytic) electron-hole exchange interaction also contributes to this splitting [20, 23–25], and this correction will result from our calculation (cf. Ref. [20]).

As our starting point we will take Eq. (17) and modify it to account for the wurtzite crystal structure as follows [20]:

$$|exc, +1^{H_j}, j\rangle = \sum_{m,n} C_m^{H_j} \phi^{(\alpha_j)}(r_e/R_j, R_j) \mathcal{R}_{n, \mathcal{F}_z - m}^{(\alpha_j)}(\mathbf{r}_h, R_j) |\Gamma_6, m\rangle |\Gamma_8, n\rangle, \quad (37)$$

where we keep the notations pertinent to the irreducible representations of the group T_d for the Bloch functions at the band extrema, and $H_j = U_j, L_j$. The coefficients $C_m^{H_j}$ are given by [20, 36]

$$C_{1/2}^{U_j, L_j} = \mp \sqrt{\frac{\sqrt{f_j^2 + d_j} \pm f_j}{2\sqrt{f_j^2 + d_j}}},$$

$$C_{-1/2}^{U_j, L_j} = \sqrt{\frac{\sqrt{f_j^2 + d_j} \mp f_j}{2\sqrt{f_j^2 + d_j}}},$$

where $f_j = -\eta_j + \Delta_j/2$, $d_j = 3\eta_j^2$,

$$\eta_j = \left(\frac{a_B}{R_j}\right)^2 \chi^{(\alpha_j)}(\beta) \hbar\omega_{TF},$$

$$\hbar\omega_{TF} = \frac{2}{\pi} \left(\frac{a_0}{a_B}\right)^3 \varepsilon_{exch},$$

a_0 is the lattice constant, ε_{exch} is the exchange constant,

$$\chi^{(\alpha)}(\beta) = \frac{1}{6} \frac{1}{1-\alpha} \cos^2 \frac{\pi\alpha}{1-\alpha}$$

$$\times \int_{\alpha}^1 dx \left[\sin \frac{\pi x}{1-\alpha} - \tan \frac{\pi\alpha}{1-\alpha} \cos \frac{\pi x}{1-\alpha} \right]^2 \left[f_0^{(\alpha)2}(x) + \frac{1}{5} f_2^{(\alpha)2}(x) \right],$$

$\Delta_j = \Delta_{cr} v^{(\alpha_j)}(\beta)$, Δ_{cr} is the bulk crystal field splitting,

$$v^{(\alpha)}(\beta) = \int_{\alpha}^1 dx x^2 \left[f_0^{(\alpha)2}(x) - \frac{3}{5} f_2^{(\alpha)2}(x) \right].$$

For $\beta = 0.275$, $\alpha = 0.68$, $v^{(\alpha)}(\beta) \approx 0.26$, $\chi^{(\alpha)}(\beta) \approx 0.35$.

The short-range (analytic) electron-hole exchange interaction and the crystal field lead to the following modifications of the exciton resonant frequencies:

$$\delta\omega_{U_j, L_j} = 2\eta_j \pm \sqrt{4\eta_j^2 + \Delta_j^2/4 - \eta_j \Delta_j}.$$

Further renormalization of the exciton resonant frequencies occurs due to the exciton interaction with the longitudinal and transverse components of the Maxwell electric field. The resulting frequencies can be found from Eq. (14) with $i, j = 1, +1^{U_1}; 1, +1^{L_1}; 2, +1^{U_2}; 2, +1^{L_2}$. Below we will omit “+1” and label the states by j, H_j with $j = 1, 2$ being the number of the semiconductor layer, and $H_j = U_j, L_j$. The matrix elements entering Eq. (14) can be expressed with the help of the Wigner $3jm$ -symbols:

$$\Xi^{i, H_i; j, H_j} = 3 \Xi^{i, j} \sum_{m, m'} C_m^{H_i} C_{m'}^{H_j} \begin{pmatrix} \frac{1}{2} & \frac{3}{2} & 1 \\ m & 1-m & -1 \end{pmatrix} \begin{pmatrix} \frac{1}{2} & \frac{3}{2} & 1 \\ m' & 1-m' & -1 \end{pmatrix}, \quad (38)$$

where $\Xi^{i, j}$ is determined by Eqs. (26), (27), and (28).

In Fig. 6 are shown real and imaginary parts of the renormalized exciton resonant frequencies as functions of the detuning defined as $\Delta\omega = \omega_{U_1} + \Re \Xi^{1, U_1; 1, U_1} - \omega_{U_2} - \Re \Xi^{2, U_2; 2, U_2}$. The structure parameters are the same with these used for Fig. 2 except that the semiconductor

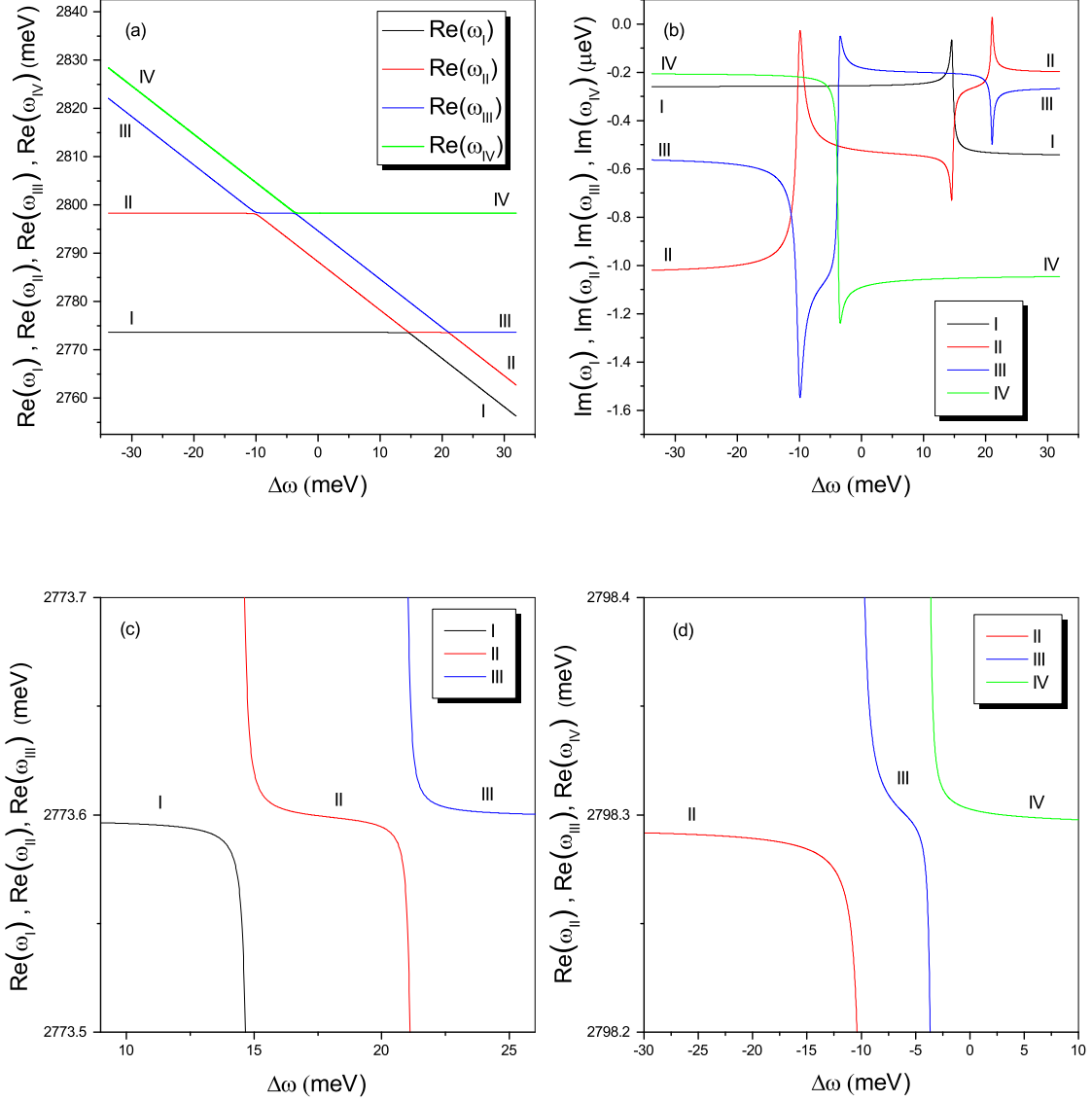


FIG. 6: (Color online). Emergence of superradiant state in a structure with two layers of wurtzite semiconductor: (a) Real parts of the renormalized frequencies as functions of the detuning from the resonance conditions between the upper energy levels in two semiconducting layers with wurtzite crystal structure. (b) Imaginary parts of the renormalized frequencies as functions of the detuning. (c),(d) Same as (a) but scaled differently.

layers have wurtzite crystal lattice. The energy positions of the exciton levels in the core layer almost do not change with the detuning (Fig. 6,a) except for the regions where they become resonant with the exciton levels in the second semiconductor layer, where avoided crossings of the exciton levels result from the inter-layer coupling via the Maxwell electric

field (Figs. 6,c,d). From Fig. 6,b one can see that, far from the resonances, the upper exciton level in the core semiconductor layer has stronger oscillator strength than the lower level while for the second semiconductor layer, one has the opposite situation. Therefore, for the resonance between the upper exciton level in the core layer and the lower exciton level in the second semiconductor layer the superradiance behavior is most pronounced. Yet, one can see a clear manifestation of the superradiance for all the four resonances. The widths of the resonances are of the same order of magnitude as in Fig. 2.

V. CONCLUDING REMARKS

When considering superradiance for atoms or molecules, one often imagines a system of identical dipole moments emitting light on the same frequency. For an ensemble of quantum dots, however, one has to account for the inhomogeneous broadening, as quantum dots are not perfect. So, if one wants to study a phenomenon occurring at resonant conditions, the width of this resonance becomes an important factor. The situation is similar if, instead of quantum dots, one has concentric spherical semiconductor layers.

In fact, an atomic or molecular system is also not free from the inhomogeneous broadening. This broadening stems from the dipole-dipole, or Van der Waals interaction which makes observation of the superradiance in systems with linear dimensions smaller than the wavelength of light and number of emitters $N > 2$, envisioned by Dicke [1], impossible, unless the dipoles are spatially arranged in some special ways [2] which leave the dipole-dipole interactions invariant under dipole permutations.

In Sec. II we proposed a system of dipole emitters in the form of concentric spherical layers of semiconductor with a simple band structure. These layers interact only via the common electro-magnetic field of light, as their dipole-dipole interaction is forbidden by the symmetry. Although the layers have different geometry, the exciton state in each individual layer has the same radiative lifetime. This allowed us to derive a simple equation, Eq. (16), showing that a symmetric state of N such distributed dipoles, one of which is excited, has a radiative lifetime N times shorter than the lifetime of an individual dipole, while the size of the system remains less than the wavelength of light. In other words, this system provides an ideal realization of the superradiance as it was proposed by Dicke [1]. However, in practice, it is extremely difficult to meet the resonance conditions necessary for observation of the

superradiance even for two layers of semiconductor with a simple band structure, as the width of the resonance is of the order of the exciton radiative linewidth, which is typically of the order of $1 \mu\text{eV}$.

In our formalism, the interaction between the layers of semiconductor with a simple band structure via the common electro-magnetic field of light is described by a purely imaginary matrix element. We saw in Sec. III that, if this matrix element acquires an appreciable real part, the width of the resonance can be made substantially broader. To this end, in Sec. III we considered a nanostructure with two layers of cubic semiconductor with a complex valence-band structure, for which the dipole-dipole interaction between the layers is no longer forbidden by the symmetry. It is interesting to note that essentially the same dipole-dipole interaction, that destroys superradiance in atomic and molecular systems, can facilitate its observation for semiconductor nanostructures. We demonstrated that, for realistic parameters, the width of the resonance can be made broader than the exciton radiative linewidth by more than two orders of magnitude. As a prototype semiconductor we chose CdSe with zinc-blende crystal lattice. This is the polytype of CdSe not found in bulk but possible in nanostructures.

To further emphasize the difference in the nature of inhomogeneous broadening and the role of the dipole-dipole interaction for superradiance in atomic and semiconductor systems, we concluded Sec. III by considering a structure with three semiconductor layers. At first glance, this structure appears to be analogous to the system of three atoms forming a triangle with a base smaller than the other sizes which was used in Ref. [2] as the simplest example of a system, where the dipole-dipole interaction destroys superradiance. However, for a structure with three concentric spherical semiconductor layers, the superradiant state of three emitters can be readily achieved, as we demonstrated in Sec. III.

In Sec. IV we considered nanostructures with two wurtzite semiconductor layers, where exciton levels excited in a given circular polarization are split by the crystal field and the electron-hole exchange interaction. We showed that observation of superradiance is possible when the resulting exciton sublevel in one semiconductor layer is brought in resonance with any of its counterparts in the other layer.

VI. ACKNOWLEDGEMENT

The author wishes to thank A.N. Poddubny for critical reading of the manuscript. This work was supported by the National Science Foundation and the Russian Foundation for Basic Research.

Appendix A: Electron wave function

The envelope wave function for the ground state of an electron confined in the spherical layer with infinitely high potential barriers, the outer radius R_2 and the inner radius $r_2 = \alpha R_2$ (see Fig. 1) has the form

$$\varphi^{(\alpha)}(x, R_2) = \frac{1}{\sqrt{2\pi} R_2^{3/2}} \frac{1}{\sqrt{1-\alpha}} \cos \frac{\pi \alpha}{1-\alpha} \left[\frac{\sin \frac{\pi x}{1-\alpha}}{x} - \tan \frac{\pi \alpha}{1-\alpha} \frac{\cos \frac{\pi x}{1-\alpha}}{x} \right] \theta(1-x) \theta(x-\alpha), \quad (\text{A1})$$

where $x = r/R_2$ and the boundary conditions of the vanishing wave function have been applied. The confinement energy is

$$E_e^{(\alpha)}(R_2) = \frac{\hbar^2 \pi^2}{2 m_e R_2^2 (1-\alpha)^2}, \quad (\text{A2})$$

where m_e is the electron effective mass.

The envelope wave function and energy of an electron confined within a sphere of radius R_1 (see Fig. 1) are given by $\varphi^{(0)}(r/R_1, R_1)$ and $E_e^{(0)}(R_1)$, respectively. Thus, at first approximation, the resonance conditions for the structure with two semiconductor layers in the context of Sec. II are reached when $R_1 = R_2(1-\alpha)$. For example, if $R_2 = 80 \text{ \AA}$, $\alpha = 0.75$, we obtain $R_1 = 20 \text{ \AA}$, $r_2 = 60 \text{ \AA}$.

Appendix B: Hole wave function

The ground state of a hole from the Γ_8 band of a cubic semiconductor confined in the spherical layer with infinitely high potential barriers, the outer radius R_2 and the inner radius $r_2 = \alpha R_2$ (see Fig. 1) can be characterized by the hole total angular momentum $F = 3/2$ and its projection, F_z , onto the z axis. The wave function of this state is given by

$$\psi_{F_z}^{(\alpha)}(\mathbf{r}, R_2) = \sum_n \mathcal{R}_{n, F_z}^{(\alpha)}(\mathbf{r}, R_2) |\Gamma_8, n\rangle, \quad (\text{B1})$$

where the components of the matrix $\hat{\mathcal{R}}^{(\alpha)}(\mathbf{r}, R_2)$ can be expressed through Wigner $3jm$ symbols [20]

$$\mathcal{R}_{n,F_z}^{(\alpha)}(\mathbf{r}, R_2) = R_2^{-3/2} \sum_{L=0,2} f_L^{(\alpha)}\left(\frac{r}{R_2}\right) (-1)^{3/2-L/2+F_z} 2 \sum_M \begin{pmatrix} \frac{3}{2} & L & \frac{3}{2} \\ n & M & -F_z \end{pmatrix} Y_{LM}\left(\frac{\mathbf{r}}{r}\right) \quad (\text{B2})$$

and Y_{LM} are the spherical harmonics with phases chosen as in Ref. [37]. The radial wave function, $f_L^{(\alpha)}(x)$, for $\alpha \leq x \leq 1$ has the form

$$f_L^{(\alpha)}(x) = C j_L(\phi_\alpha x) + D n_L(\phi_\alpha x) + (-1)^{L/2} A j_L(\sqrt{\beta} \phi_\alpha x) + (-1)^{L/2} B n_L(\sqrt{\beta} \phi_\alpha x), \quad (\text{B3})$$

where $j_L(x)$ and $n_L(x)$ are the spherical Bessel functions, β is the light to heavy hole effective mass ratio, the coefficients A , B , C , and D satisfy the following system of equations

$$A j_0(\alpha \sqrt{\beta} \phi_\alpha) + B n_0(\alpha \sqrt{\beta} \phi_\alpha) + C j_0(\alpha \phi_\alpha) + D n_0(\alpha \phi_\alpha) = 0, \quad (\text{B4})$$

$$A j_2(\alpha \sqrt{\beta} \phi_\alpha) + B n_2(\alpha \sqrt{\beta} \phi_\alpha) - C j_2(\alpha \phi_\alpha) - D n_2(\alpha \phi_\alpha) = 0, \quad (\text{B5})$$

$$A j_0(\sqrt{\beta} \phi_\alpha) + B n_0(\sqrt{\beta} \phi_\alpha) + C j_0(\phi_\alpha) + D n_0(\phi_\alpha) = 0, \quad (\text{B6})$$

$$A j_2(\sqrt{\beta} \phi_\alpha) + B n_2(\sqrt{\beta} \phi_\alpha) - C j_2(\phi_\alpha) - D n_2(\phi_\alpha) = 0, \quad (\text{B7})$$

and ϕ_α is obtained from the condition that the corresponding determinant vanishes. The functions $f_L^{(\alpha)}(x)$ are normalized by the condition

$$\int_{\alpha}^1 \left\{ \left[f_0^{(\alpha)}(x) \right]^2 + \left[f_2^{(\alpha)}(x) \right]^2 \right\} x^2 dx = 1.$$

The confined hole energy is

$$E_h^{(\alpha)}(R_2) = \frac{\hbar^2 \phi_\alpha^2 (\gamma_1 - 2\gamma)}{2 m_0 R_2^2}, \quad (\text{B8})$$

where m_0 is the free electron mass.

When $\beta \rightarrow 1$ the light and heavy hole subbands of the valence band become degenerate. In this case, for the hole ground state, Eqs. (B4) – (B7) yield

$$j_0(\alpha \phi_\alpha) n_0(\phi_\alpha) - n_0(\alpha \phi_\alpha) j_0(\phi_\alpha) = 0$$

or

$$\tan \phi_\alpha = \tan(\alpha \phi_\alpha),$$

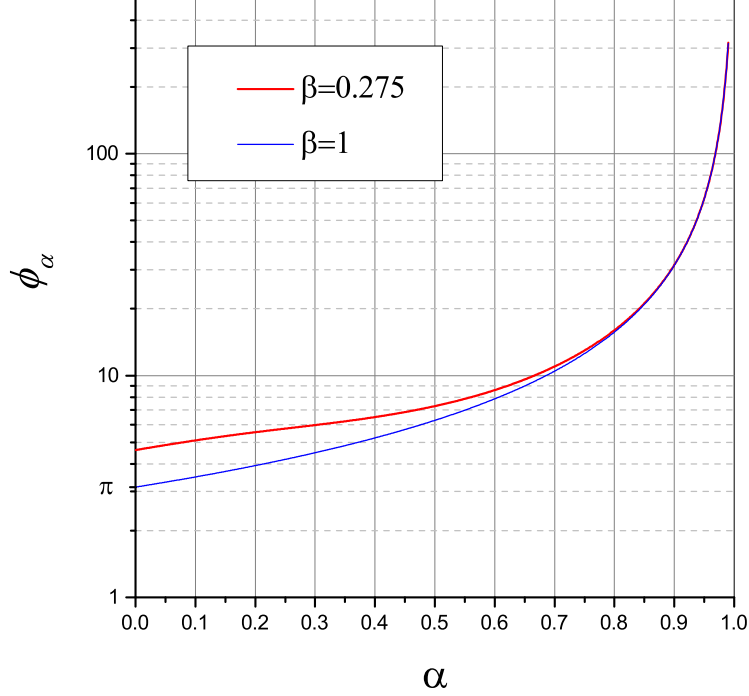


FIG. 7: (Color online). Dependence of ϕ_α on α for $\beta = 0.275$ (red line, top curve) and for $\beta = 1$ (blue line, bottom curve).

$A = C$, and $B = D$. Therefore, in this limit $\phi_\alpha = \pi/(1 - \alpha)$, $f_2^{(\alpha)}(x) = 0$, and $f_0^{(\alpha)}(x) = R_2^{3/2} \varphi^{(\alpha)}(x, R_2)$ [cf. Eqs. (A1), (A2)].

When $\alpha = 0$ then $B = D = 0$ and Eqs. (B6), (B7) yield

$$j_0(\sqrt{\beta} \phi_0) j_2(\phi_0) + j_2(\sqrt{\beta} \phi_0) j_0(\phi_0) = 0.$$

This is the case of the hole confined in a sphere. However, one should be careful with this limiting case, as, for the hole confined in a sphere, $f_0^{(0)}(x = 0) \neq 0$.

In Fig. 7 ϕ_α is plotted as a function of α for $\beta = 0.275$ and $\beta = 1$. The value of $\beta = 0.275$ gives the ratio of the light- to heavy-hole effective masses for CdSe while the value of $\beta = 1$ corresponds to degenerate light and heavy hole subbands when analytic results of Appendix A become applicable and $\phi_\alpha = \pi/(1 - \alpha)$.

Appendix C: Values of CdSe material parameters used in the calculations

We chose CdSe as a prototype semiconductor for illustrative purposes. In Table I we list parameters used in our numerical calculations.

TABLE I: Values of CdSe material parameters used in the calculations [25, 36]

parameter	value	units	parameter	value	units
E_g	1.74	eV	ε_b	5.7	–
m_e	0.11	m_0	$\hbar\omega_{LT}$	0.95	meV
γ_1	2.04	m_0	a_B	56	Å
γ	0.58	m_0	$\hbar\omega_{TF}$	124	μeV
β	0.275	–	Δ_{cr}	25	meV

-
- [1] R.H. Dicke, Coherence in Spontaneous Radiation Processes, *Phys. Rev.* **93**, 99 (1954).
- [2] M. Gross and S. Haroche, Superradiance: an Essay on the Theory of Collective Spontaneous Emission, *Phys. Rep.* **93**, 301 (1982).
- [3] A.V. Andreev, V.L. Emel’yanov, and Yu.A. Il’inskii, *Cooperative Effects in Optics. Superradiance and Phase Transitions* (IOP Publishing, Bristol and Philadelphia, 1993).
- [4] L. Mandel and E. Wolf, *Optical coherence and quantum optics* (Cambridge University Press, 1995).
- [5] J.M. Raimond, P. Goy, M. Gross, C. Fabre, and S. Haroche, Statistics of Millimeter-Wave Photons Emitted by a Rydberg-Atom Maser: An Experimental Study of Fluctuations in Single-Mode Superradiance, *Phys. Rev. Lett.* **49**, 1924 (1982).
- [6] R.G. DeVoe and R.G. Brewer, Observation of Superradiant and Subradiant Spontaneous Emission of Two Trapped Ions, *Phys. Rev. Lett.* **76**, 2049 (1996).

- [7] T.V. Shahbazyan, M.E. Raikh, and Z.V. Vardeny, Mesoscopic cooperative emission from a disordered system, *Phys. Rev. B* **61**, 13266 (2000).
- [8] J.A. Mlynek, A.A. Abdumalikov, C. Eichler, and A. Wallraff, Observation of Dicke superradiance for two artificial atoms in a cavity with high decay rate, *Nat. Commun.* **5**, 5186 (2014).
- [9] R. Röhlsberger, K. Schlage, B. Sahoo, S. Couet, and R. Ruffer, Collective Lamb Shift in Single-Photon Superradiance, *Science* **328**, 1248 (2010).
- [10] G. Parascandolo and V. Savona, Long-Range Radiative Interaction between Semiconductor Quantum Dots, *Phys. Rev. B* **71**, 045335 (2005).
- [11] M. Scheibner, T. Schmidt, L. Worschech, A. Forchel, G. Bacher, T. Passow, and D. Hommel, Superradiance of Quantum Dots, *Nat. Phys.* **3**, 106 (2007).
- [12] V.I. Yukalov and E.P. Yukalova, Dynamics of quantum dot superradiance, *Phys. Rev. B* **81**, 075308 (2010).
- [13] N.S. Averkiev, M.M. Glazov, and A.N. Poddubnyi, Collective Modes of Quantum Dot Ensembles in Microcavities, *J. Exp. Theor. Phys.* **108**, 836 (2009).
- [14] D. Dorfs and A. Eychmüller, Multishell semiconductor nanocrystals, in: *Semiconductor Nanocrystal Quantum Dots: Synthesis, Assembly, Spectroscopy and Applications*, edited by A.L. Rogach (Springer, Wien 2008).
- [15] D. Battaglia, B. Blackman, and X. Peng, Coupled and Decoupled Dual Quantum Systems in One Semiconductor Nanocrystal, *J. Am. Chem. Soc.* **127**, 10889 (2005).
- [16] J. Berezovsky, O. Gywat, F. Meier, D. Battaglia, X. Peng, and D.D. Awschalom, Initialization and read-out of spins in coupled core-shell quantum dots, *Nat. Phys.* **2**, 831 (2006).
- [17] E.A. Dias, S.L. Sewall, and P. Kambhampati, Light Harvesting and Carrier Transport in Core/Barrier/Shell Semiconductor Nanocrystals, *J. Phys. Chem. C* **111**, 708 (2007).
- [18] E.A. Dias, A.F. Grimes, D.S. English, and P. Kambhampati, Single Dot Spectroscopy of Two-Color Quantum Dot/Quantum Shell Nanostructures, *J. Phys. Chem. C* **112**, 14229 (2008).
- [19] A. Teitelboim, N. Meir, M. Kazes, and D. Oron, Colloidal Double Quantum Dots, *Acc. Chem. Res.* **49**, 902 (2016).
- [20] S.V. Goupalov, P. Lavallard, G. Lamouche, and D.S. Citrin, Electrodynamical Treatment of the Electron-Hole Long-Range Exchange Interaction in Semiconductor Nanocrystals, *Phys. Sol. St.* **45**, 768 (2003).

- [21] S.V. Goupalov, Light Scattering on Exciton Resonance in a Semiconductor Quantum Dot: Exact Solution, *Phys. Rev. B* **68**, 125311 (2003).
- [22] E.L. Ivchenko, *Optical Spectroscopy of Semiconductor Nanostructures* (Alpha Science International, Harrow, UK, 2005).
- [23] S.V. Goupalov, E.L. Ivchenko, and A.V. Kavokin, Anisotropic Exchange Splitting of Excitonic Levels in Small Quantum Systems, *Superlatt. Microstruct.* **23**, 1205 (1998).
- [24] S.V. Goupalov and E.L. Ivchenko, Electron-Hole Long-Range Exchange Interaction in Semiconductor Quantum Dots, *J. Cryst. Growth* **184/185**, 393 (1998).
- [25] S.V. Goupalov and E.L. Ivchenko, The Fine Structure of Excitonic Levels in CdSe Nanocrystals, *Phys. Sol. St.* **42**, 1976 (2000).
- [26] C. Sinito, M.J. Fernée, S.V. Goupalov, P. Mulvaney, P. Tamarat, and B. Lounis, Tailoring the Exciton Fine Structure of Cadmium Selenide Nanocrystals with Shape Anisotropy and Magnetic Field, *ACS Nano* **8**, 11651 (2014).
- [27] M.J. Fernée, P. Tamarat, B. Lounis, Spectroscopy of Single Nanocrystals, *Chem. Soc. Rev.* **43**, 1311 (2014).
- [28] X. Brokmann, L. Coolen, M. Dahan, J.P. Hermier, Measurement of the Radiative and Nonradiative Decay Rates of Single CdSe Nanocrystals through a Controlled Modification of their Spontaneous Emission, *Phys. Rev. Lett.* **93**, 107403 (2004).
- [29] L.D. Landau and E.M. Lifshitz, *The Classical Theory of Fields* (Pergamon Press, Oxford, 1971).
- [30] E.L. Ivchenko, A.I. Nesvizhskii, and S. Jorda, Bragg reflection of light from quantum-well structures, *Phys. Sol. St.* **36**, 1156 (1994).
- [31] M.J. Fernée, C. Sinito, Y. Louyer, C. Potzner, T.-L. Nguyen, P. Mulvaney, P. Tamarat, B. Lounis, Magneto-optical Properties of Trions in Non-blinking Charged Nanocrystals Reveal an Acoustic Phonon Bottleneck, *Nat. Commun.* **3**, 1287 (2012).
- [32] H. Qin, Y. Niu, R. Meng, X. Lin, R. Lai, W. Fang, and X. Peng, Single-Dot Spectroscopy of Zinc-Blende CdSe/CdS Core/Shell Nanocrystals: Nonblinking and Correlation with Ensemble Measurements, *J. Am. Chem. Soc.* **136**, 179 (2014).
- [33] C. Cohen-Tannoudji, J. Dupont-Roc, G. Grynberg, *Atom-Photon Interactions* (Wiley, New York, 1992).
- [34] R. Loudon, *The Quantum Theory of Light*, 3rd Ed. (Oxford University Press, New York,

- 2000).
- [35] V.M. Agranovich and M.D. Galanin, *Electronic Excitation Energy Transfer in Condensed Matter* (North-Holland, Amsterdam, 1982).
 - [36] Al.L. Efros, M. Rosen, M. Kuno, M. Nirmal, D.J. Norris, and M.G. Bawendi, Band-edge exciton in quantum dots of semiconductors with a degenerate valence band: Dark and bright exciton states, *Phys. Rev. B* **54**, 4843 (1996).
 - [37] D.A. Varshalovich, A.N. Moskalev, and V.K. Khersonskii, *Quantum Theory of Angular Momentum* (World Scientific, Singapore, 1988).